Supporting Information

Navigating Lithium Fluoride Formation by Electrode Interphase Engineering with Amphiphilic Covalent Organic Frameworks based Electrolyte

Huifen Zhuang†, Zixi Zheng†, Yafang Guan†, Runhan Li, Runhua Zuo, Wenhai Feng, Yifa Chen* and Ya-Qian Lan

Correspondence to: Email: chyf927821@163.com (Y. C.)

Materials

All solvents and reagents obtained from commercial sources were used without further purification. Acetic acid (AcOH, AR, ≥ 99.8%) were obtained from Sinopharm Chemical Reagent Co., Ltd, N,N-dimethylformamide (DMF, AR), 1-methyl 2-pyrrolidone (NMP, AR), ethanol (AR), 1,4-dioxane (AR), tetrahydrofuran (THF, 99.5%), mesitylene (MES, AR), triamino-guanidine hydrochloride (TG_{Cl}), 2,5-bis(2-methoxyethoxy)terephthalaldehyde (BMTP), 2,5-dimethoxybenzene-1,4-dicarboxaldehyde (DMTP) were obtained from Shanghai Tensus Biotech Co., Ltd. 1,4-benzenedicarboxaldehyde (BDA) were obtained from Adamas. Li chips (diameter size, 15.6 mm and thickness, 450 μm) were purchased from China Energy Lithium Co., Ltd, polyvinylidene fluoride (PVDF), Cu foil, Celgard 2500, Celgard 2325, $LiFePO_4$ and Super P were obtained from commercial sources.

Materials characterizations

Powder X-ray diffraction (PXRD) patterns were recorded by a D/max 2500 VL/PC X-ray diffractometer (Rigaku SmartLab, Japan) under the Cu Kα radiation at 40 kV, 15 mA. Fourier transform infrared spectrometry (FT-IR) spectra were investigated by a Thermo Nicolet IS50 FT-IR spectrometer ranged from 4000 to 400 cm^{-1} with KBr pellets under ambition conditions. Solid-state ^{13}C cross-polarization/magnetic angle spinning (CP/MAS) experiment was carried out on Bruker 400 AVANCE spectrometer equipped with a 9.4 T superconducting magnet and a 4 mm double-resonance MAS probe. The ESCALAB 250Xi system from Thermo Scientific was used to record on X-ray photoelectron spectroscopy (XPS) measurements. All XPS spectra were conducted by the C1s peak at 284.8 eV. Nitrogen adsorption-desorption isotherm was identified using a Quantachrome Autosorb-IQ2 at 77 K. Morphological and structural characterizations were carried out through high-resolution transmission electron microscopy (HRTEM JEOL JEM-F200, 200 kV) and a field-emission scanning electron microscope (SEM, Hitachi SU-8010) system with energy-dispersive spectral (EDS) analysis instrument.

Experimental Procedures

Synthesis Method

Synthesis of TGBM-COF

7.0 mg TG_{Cl}, 21.2 mg BMTP and the mixed solution of mesitylene (0.2 mL), tetrahydrofuran (0.8 mL) and 6 M HAc (0.1 mL) were added into a Pyrex tube. After sonicating for 15 min, the Pyrex tube was conducted by three freeze-pump-thaw cycles in a N_2 liquid bath (77 K) and then sealed under vacuum. After heating at 150 °C for 3 days, the orange sample was filtrated and then washed with tetrahydrofuran. Then, the sample was further washed with tetrahydrofuran in a Soxhlet extractor for 24 h. Finally, the product was obtained after evacuating at 60 °C under vacuum overnight.

Synthesis of TGDM-COF

7.0 mg TG_{Cl}, 14.5 mg DMTP and the mixed solution of mesitylene (0.5 mL), tetrahydrofuran (0.5 mL) and 3 M HAc (0.1 mL) were added in a Pyrex tube. The following treatment was similar as that of TGBM-COF. After heating at 150 °C for 3 days, the orange sample was collected by filtration and washed with tetrahydrofuran, and further transferred to a Soxhlet extractor and washed with tetrahydrofuran for 24 h. Finally, the product was obtained after evacuating at 60 °C under vacuum overnight.

Synthesis of TGBD-COF

14.0 mg TG_{Cl}, 20.1 mg BDA and the mixed solution of mesitylene (0.9 mL), 1,4-dioxane (0.1 mL) and 6 M HAc (0.1 mL) were added in a Pyrex tube. The following treatment was

similar as that of TGBM-COF. After heating at 150 °C for 3 days, the yellow sample was filtrated and then washed with tetrahydrofuran, and further washed with tetrahydrofuran in a Soxhlet extractor for 24 h. Finally, the product was obtained after evacuating at 60 °C under vacuum overnight.

Preparation of electrolyte

The 0.1% TGBM-COF electrolyte was prepared in an argon-filled glovebox (H_2O and O_2 content level < 0.01 ppm) by dispersing TGBM-COF into blank electrolyte. Blank electrolyte is 1.0 M lithium hexafluorophosphate ($LiPF_6$) dissolved in ethylene carbonate (EC), dimethyl carbonate (DMC) and ethyl methyl carbonate (EMC) with a volume ratio of 1: 1: 1. In detail, 11.0 mg TGBM-COF powder (after 30 min ball-milling) was added to the 10 mL blank electrolyte, followed by vigorous stirring for 3 h to obtain a uniform dispersion. Similarly, the 0.1% TGDM-COF and 0.1% TGBD-COF were obtained through the same procedures.

Electrochemical measurements

Electrochemical behaviors of the electrolyte additives were measured by using CR2032 type coin cells in an argon-filled glove box, where the water and oxygen contents were both lower than 0.01 ppm. The thickness of Li anode is 450 μm. All the assembled batteries were operated in 60 μL 1.0 M $LiPF_6$ in EC/EMC/DMC (volume ratio, 1: 1: 1). For Li symmetric cells and Li||Cu half cells, Celgard 2500 was served as the separator. For full cells, the $LiFePO_4$ electrodes were made by casting the slurry consisting of $LiFePO_4$, super P, and PVDF (8: 1: 1 by mass ratio) in NMP solvent onto Al foil and dried at 80 °C under vacuum overnight. The diameter of LFP cathode is 10 mm. The average loading mass of the as-prepared LFP cathode is approximately 3 mg cm^{-2}. Celgard 2325 was served as the separator. The cells were charged and discharged between 2.5 and 4 V (vs Li^+/Li) at different current densities (1 C = 170 mA g^{-1}). All coin cells were galvanostatically cycled on a LAND battery-testing system. Both EIS and CV were performed on a Chenhua CHI-760 electrochemical workstation.

Computational methods

Density functional theory (DFT) calculations

All calculations were conducted using the DFT[1] method at the B3LYP/6-31G(d) level, employing the Gaussian 16 software.[2] Geometry optimizations were performed at the B3LYP/6-31G(d).[3-6] Frequency calculations were then carried out at the same theoretical level to confirm that the stationary points correspond to equilibrium states and to obtain the relevant thermodynamic data at 298.15 K and 1 atm. The 3D structural images were generated using the Materials Studio 2020 program.[7]

MD simulations

All molecular dynamics simulations were performed using Gromacs2018.[8] The initial simulation system was established by uniformly mixing 60 Li^+, 60 PF_6^-, 300 EC molecules, 200 EMC molecules, and 220 DMC molecules to form an electrolyte phase. The dimensions of the simulation box were 4.1 nm in the x direction, 7.2 nm in the y direction, and 13.6 nm in the z direction. Two COF layers were placed in the central area of the simulation box with a spacing of 2.4 nm. The parameters for Li^+ , EC, EMC, DMC, and PF_6^-, were determined using the Amber force field.[9] The parameters of COF are determined by the GAFF force field.[10] Three-dimensional periodic boundary conditions were applied throughout the simulation process. The van der Waals interactions were described using the Lennard-Jones (LJ) potential,[11] with a cutoff distance set at 1.2 nm. The LJ parameters between different atomic pairs were automatically determined according to the Lorentz-Berthelot mixing rule. The Coulomb interactions were calculated using the Particle Mesh Ewald (PME) method.[12] Initially, energy

minimization was conducted to relax the initial configuration. This was followed by a 20 ns production run at 298.15 K and 1 bar, employing a time step of 2 fs.

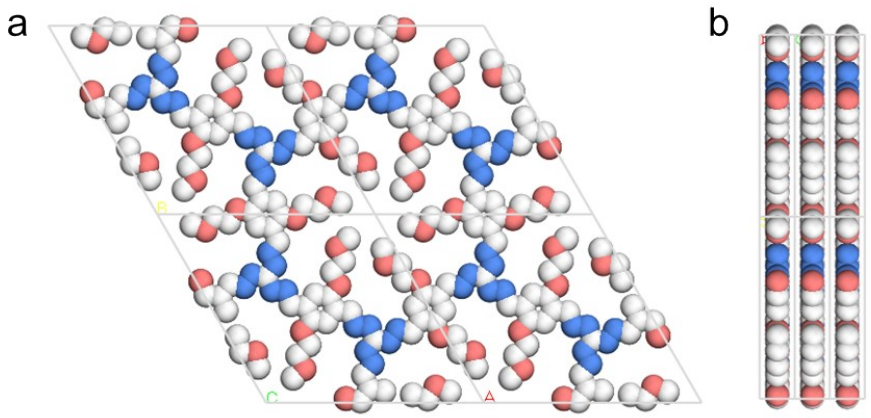

Figure S1. The simulated AA stacking mode of TGBM-COF. **a** Top view. **b** Side view.

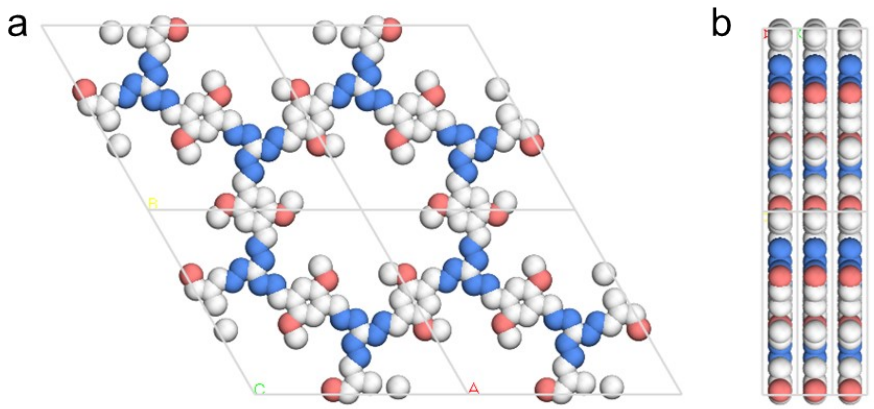

Figure S2. The simulated AA stacking mode of TGDM-COF. **a** Top view. **b** Side view.

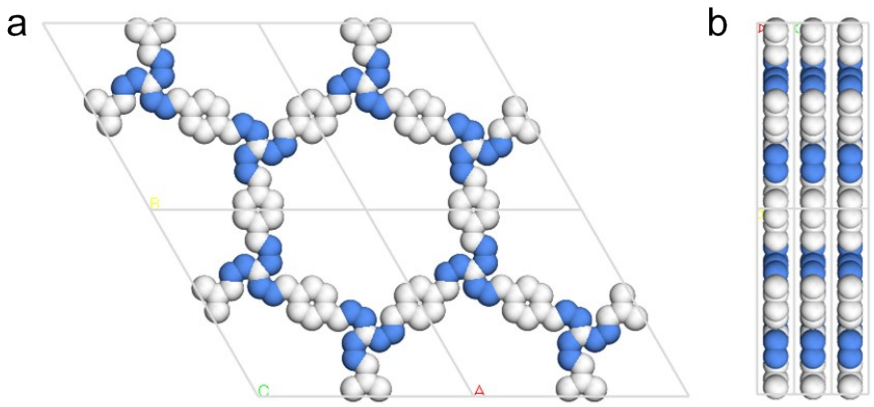

Figure S3. The simulated AA stacking mode of TGBD-COF. **a** Top view. **b** Side view.

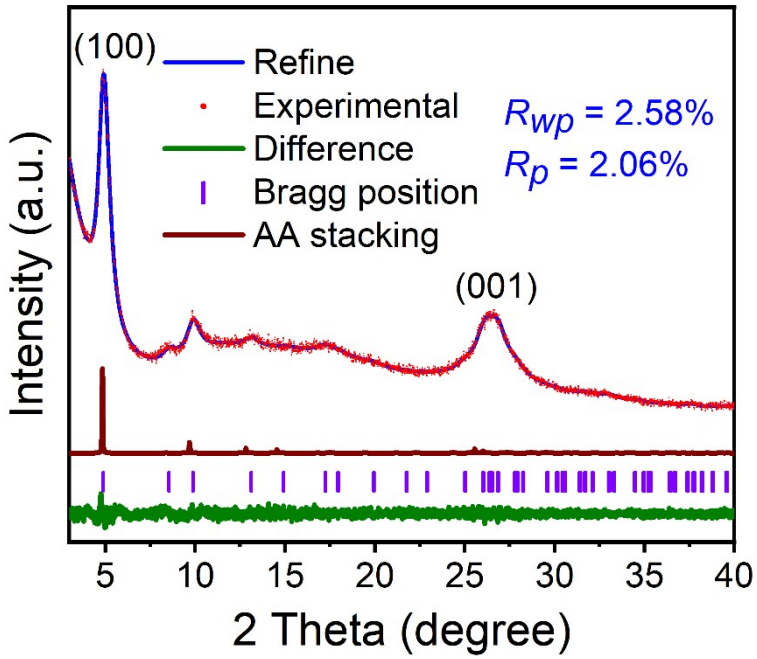

Figure S4. Experimental and simulated PXRD patterns of TGDM-COF.

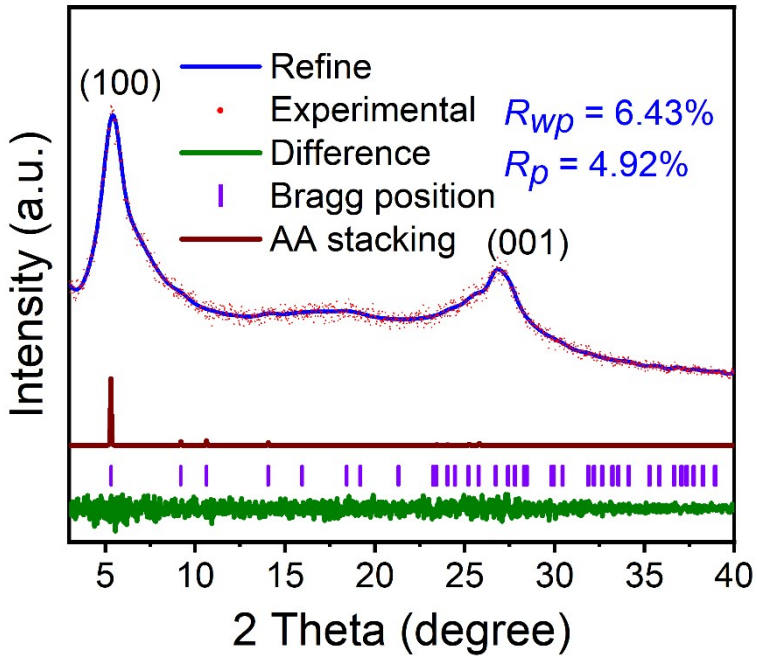

Figure S5. Experimental and simulated PXRD patterns of TGBD-COF.

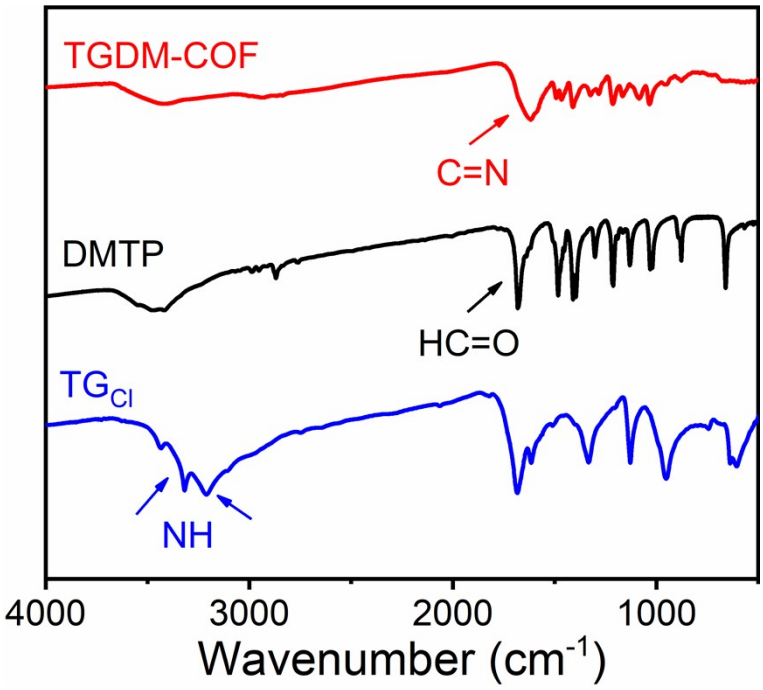

Figure S6. FT-IR spectra of TG_{Cl}, DMTP and TGDM-COF.

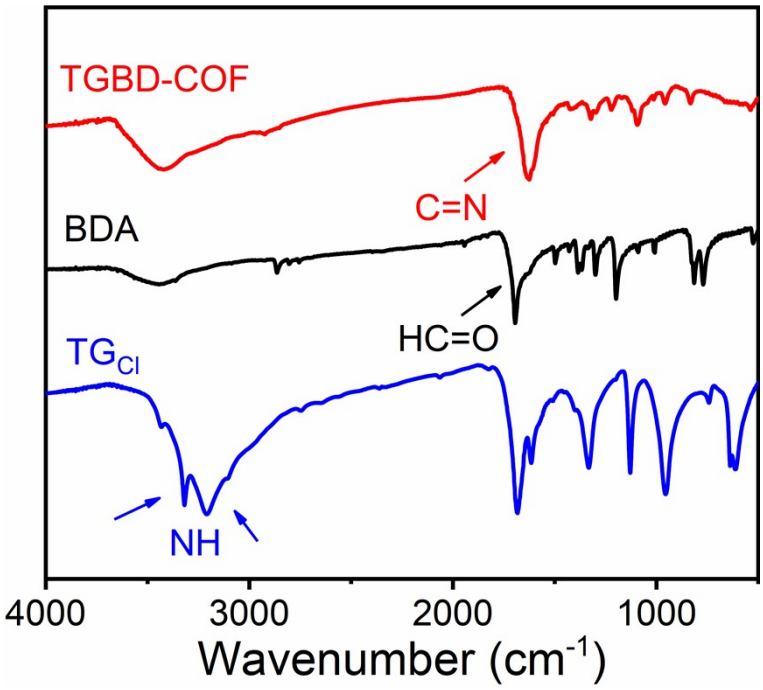

Figure S7. FT-IR spectra of TG_{Cl}, BDA and TGBD-COF.

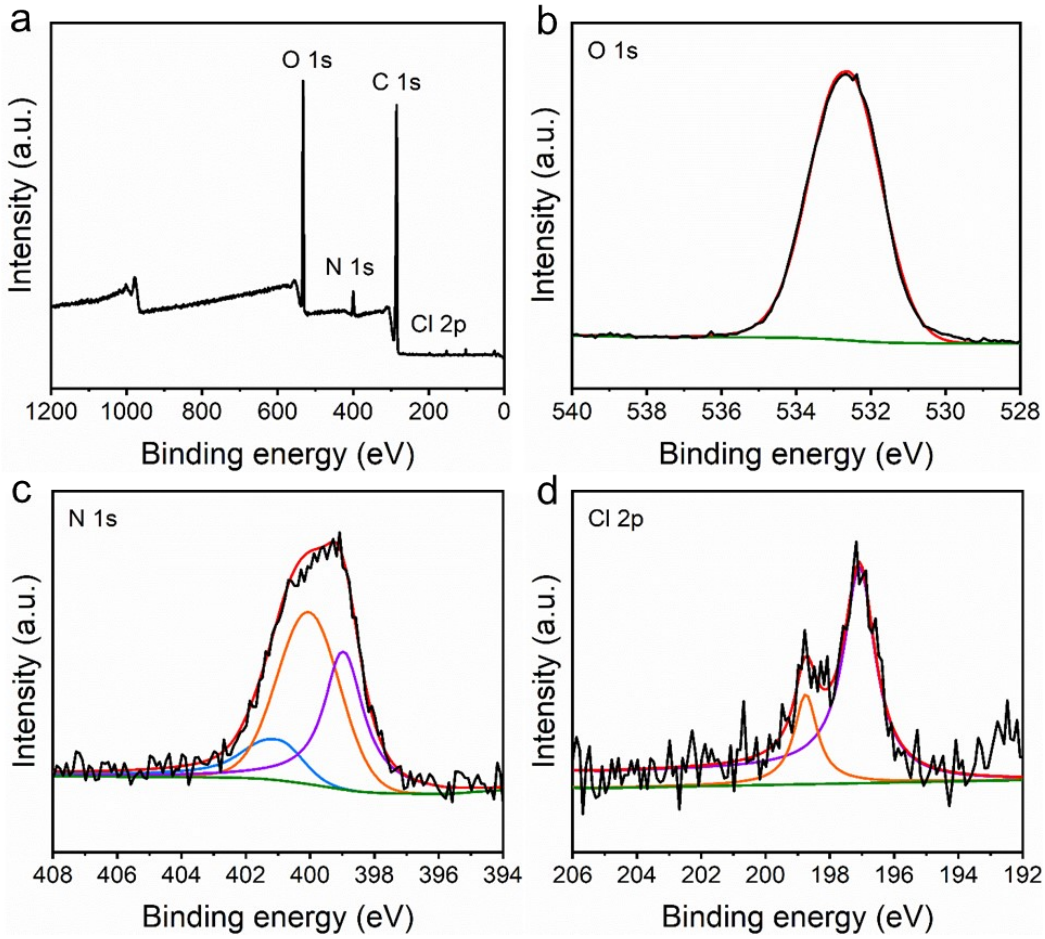

Figure S8. XPS spectra of TGBM-COF. **a** Survey scan XPS profile. **b** O 1s. **c** N 1s. **d** Cl 2p.

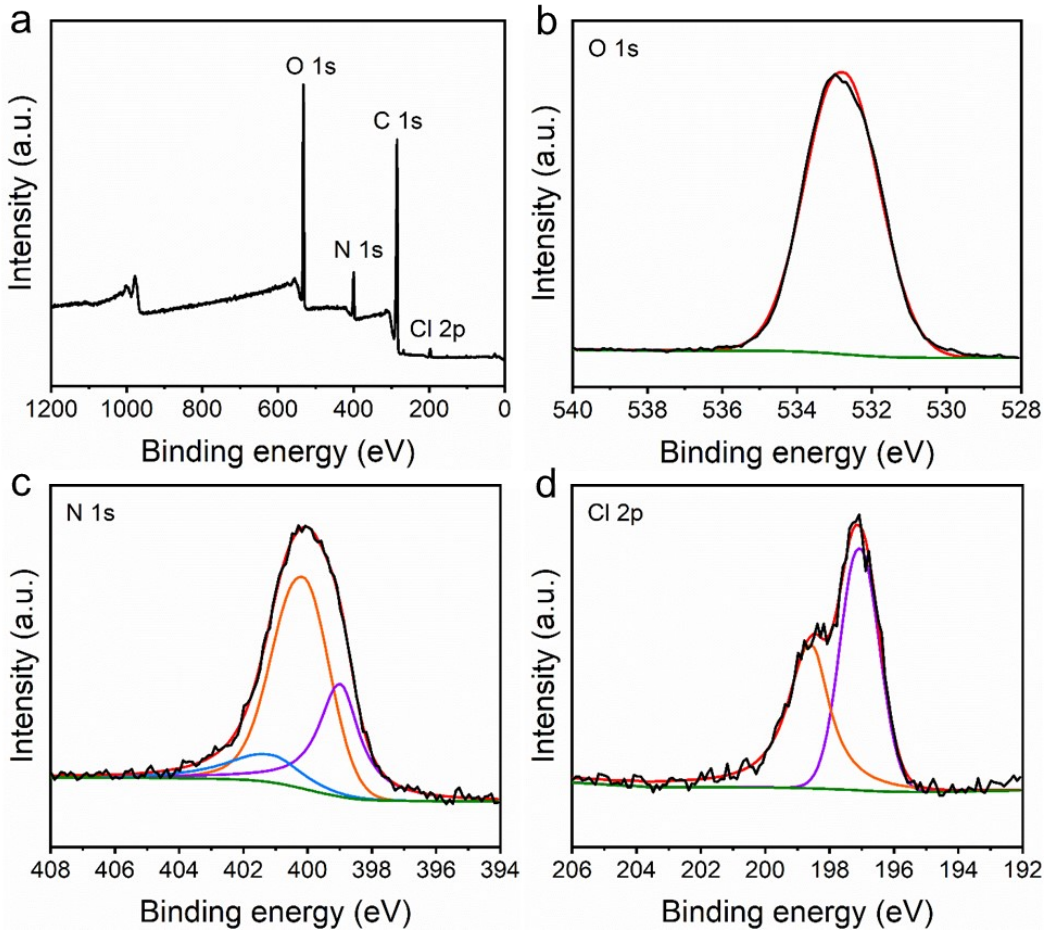

Figure S9. XPS spectra of TGDM-COF. **a** Survey scan XPS profile. **b** O 1s. **c** N 1s. **d** Cl 2p.

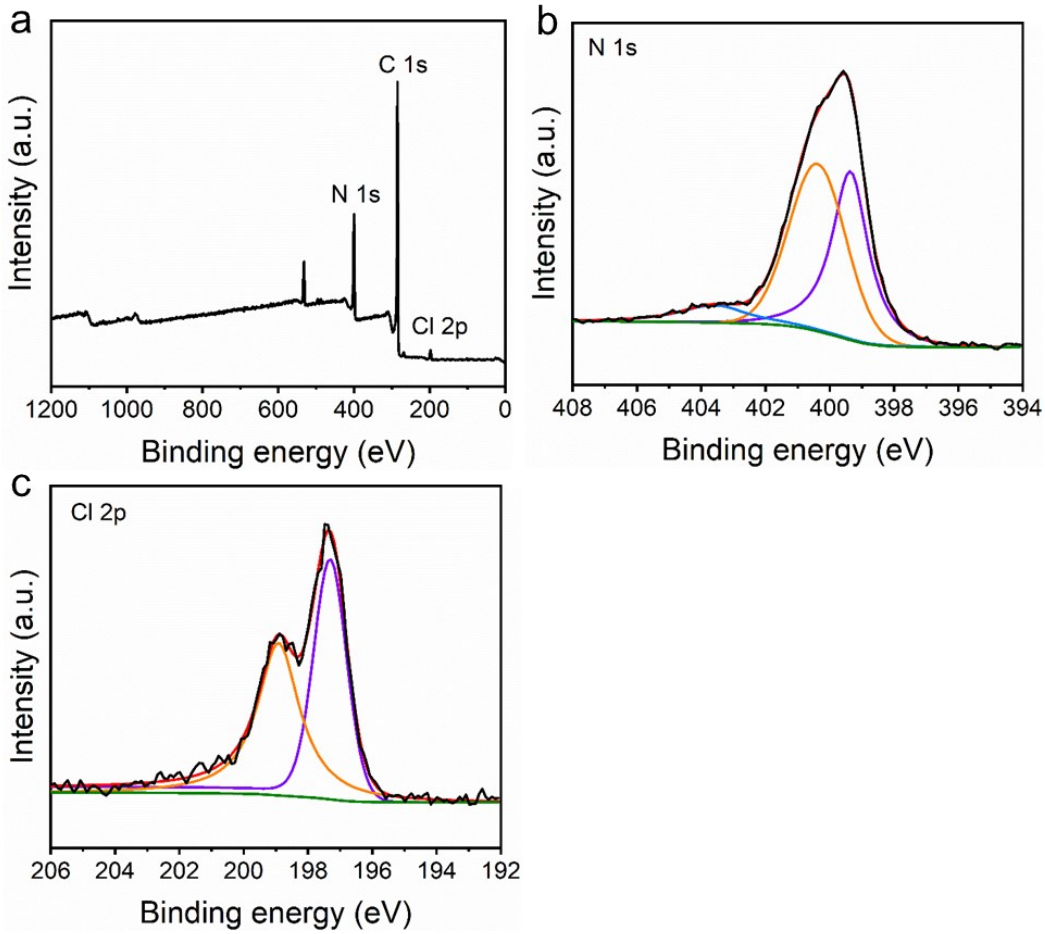

Figure S10. XPS spectra of TGBD-COF. **a** Survey scan XPS profile. **b** N 1s. **c** Cl 2p.

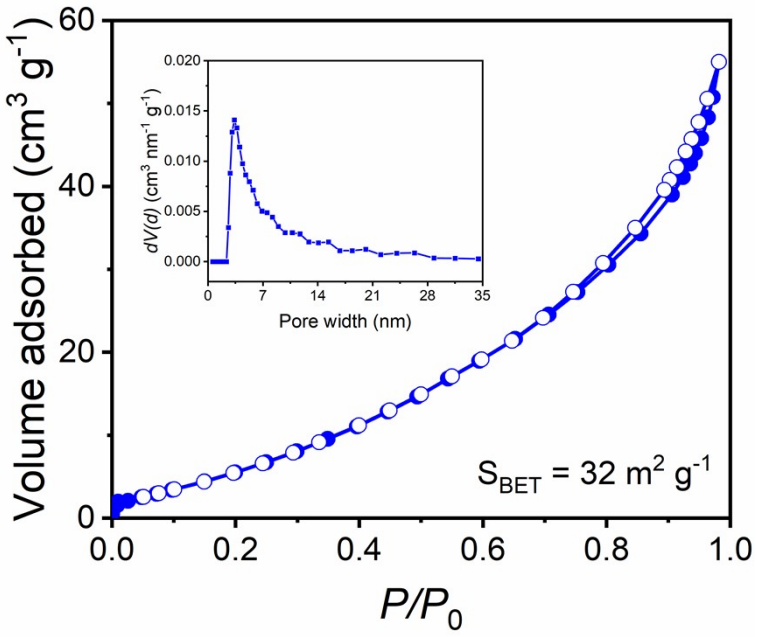

Figure S11. N_2 sorption and the pore size distribution curves of TGBM-COF at 77 K.

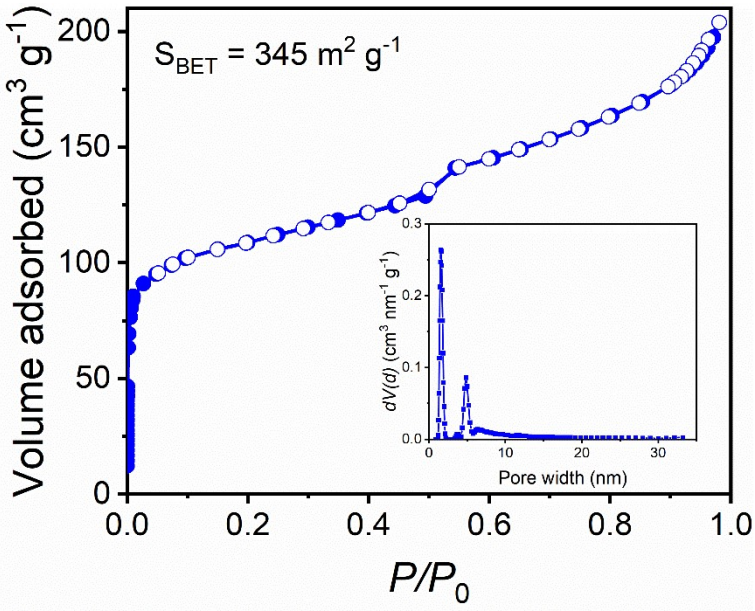

Figure S12. N_2 sorption and the pore size distribution curves of TGDM-COF at 77 K.

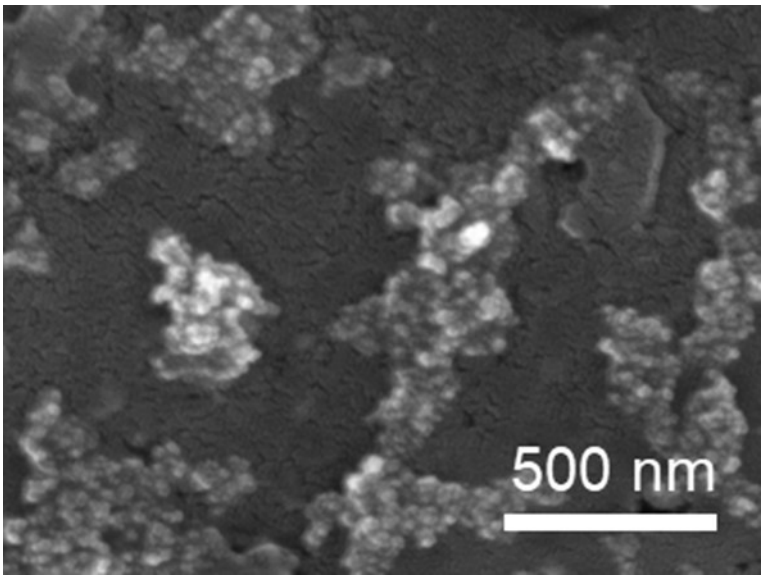

Figure S13. SEM image of TGBM-COF.

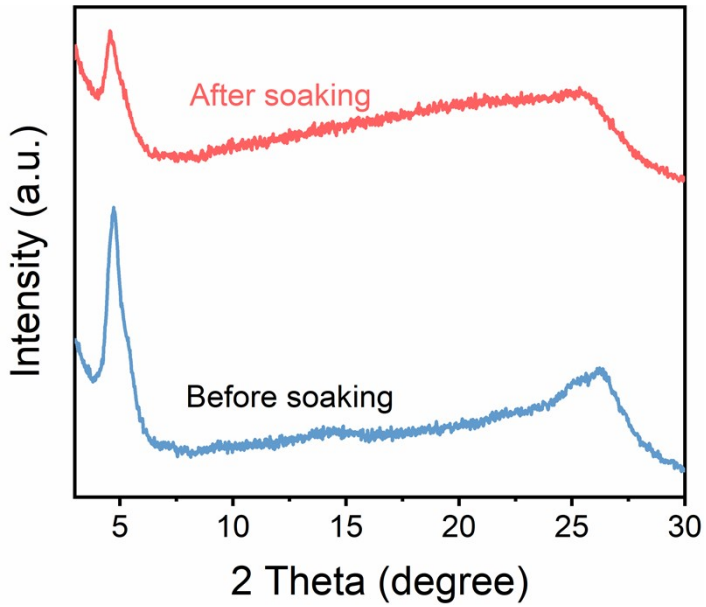

Figure S14. PXRD patterns of the stability test of TGBM-COF in electrolyte for one day.

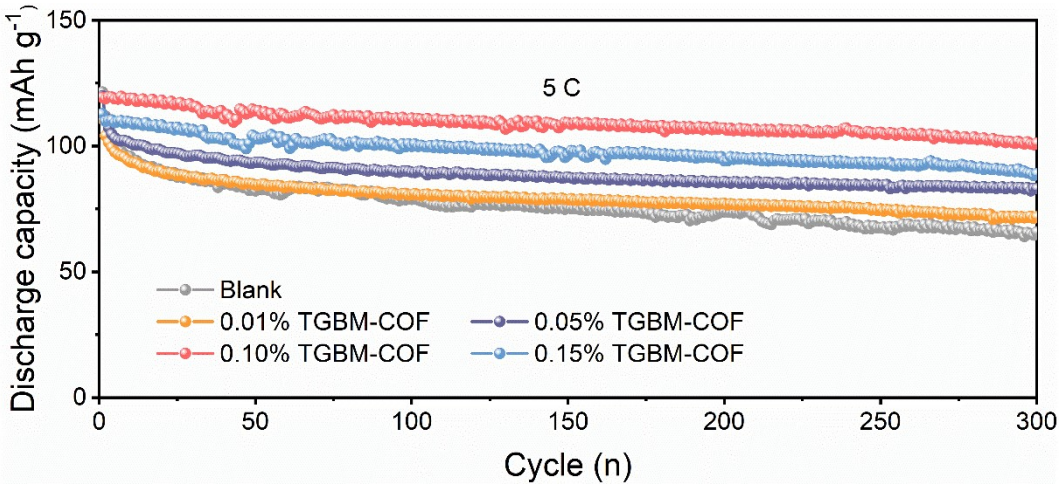

Figure S15. Electrochemical behaviors of Li||LFP full cells using electrolyte containing diferent contents of TGBM-COF at 5 C.

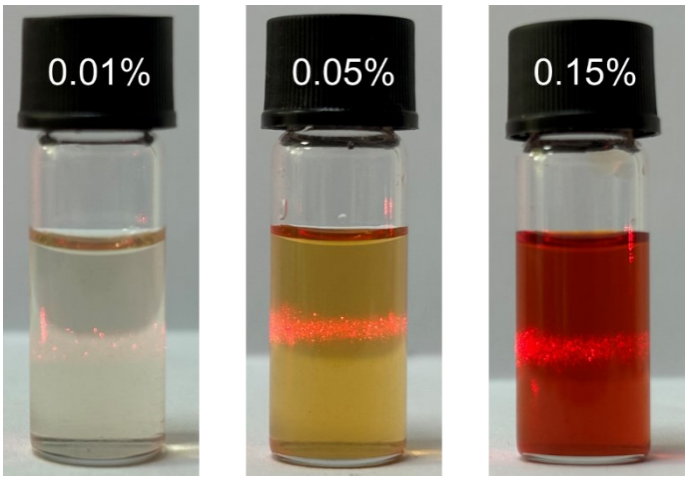

Figure S16. Tyndall effects of TGBM-COF electrolyte with different concentrations standing for one year.

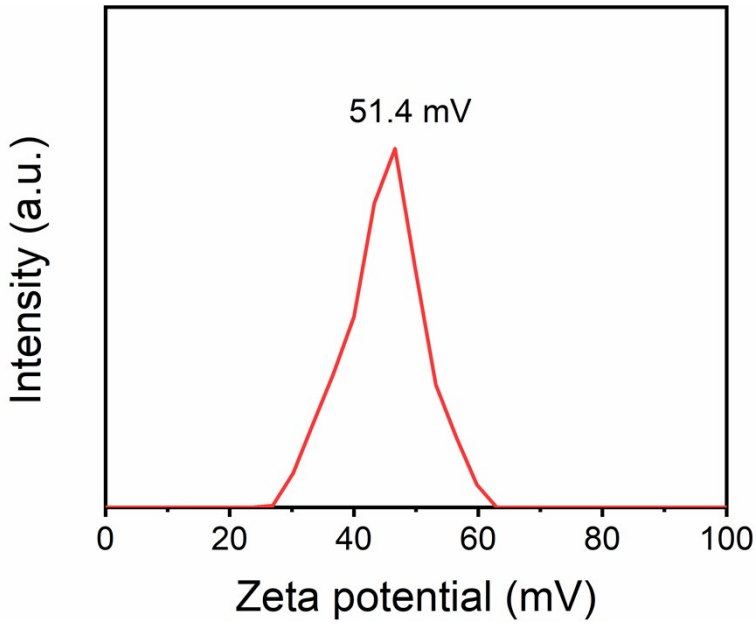

Figure S17. The Zeta potential of TGBM-COF.

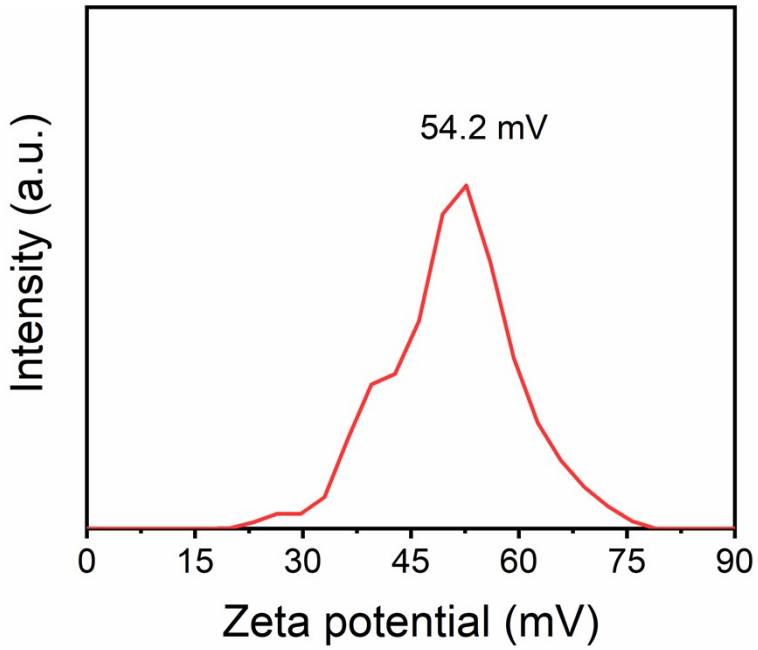

Figure S18. The Zeta potential of TGDM-COF.

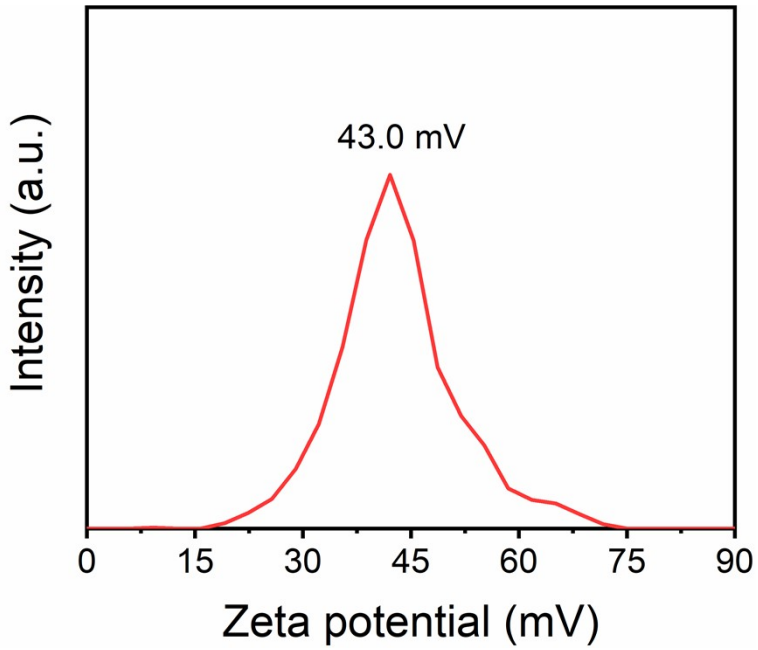

Figure S19. The Zeta potential of TGBD-COF.

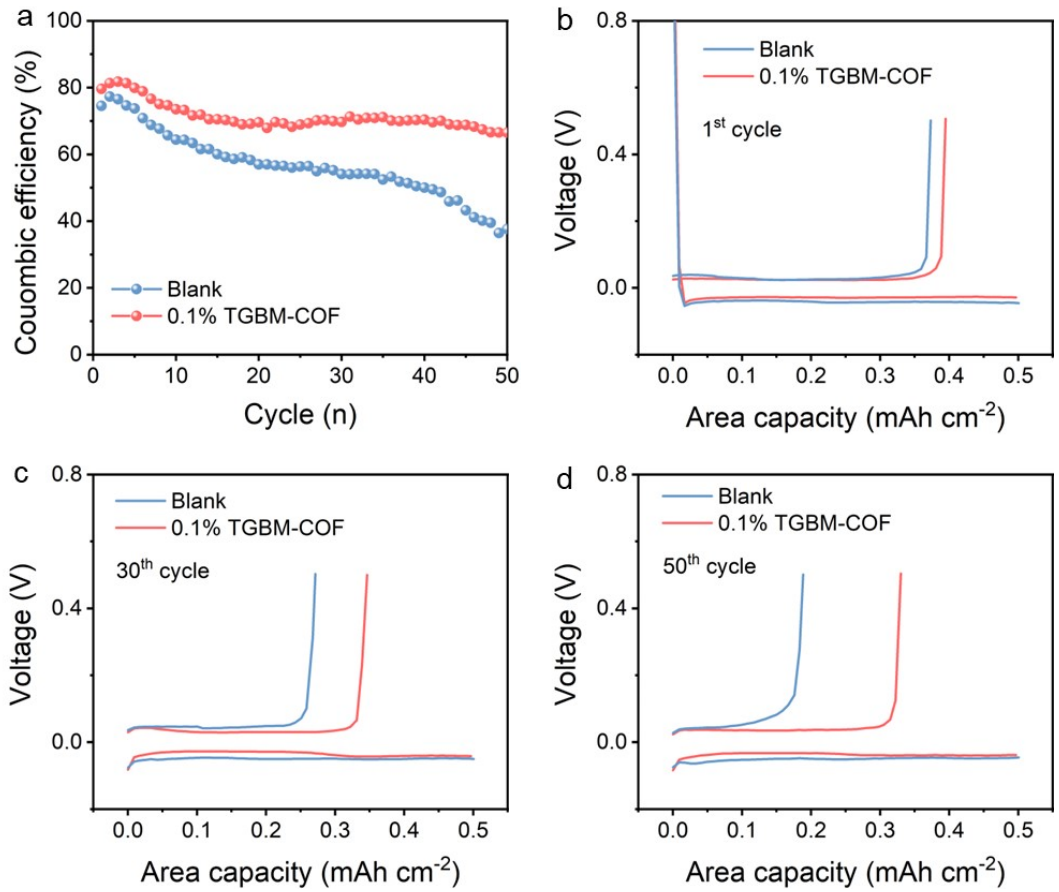

Figure S20. Coulombic efficiency of Li||Cu cells with different electrolytes at 0.5 mA cm^{-2} with 1 mAh cm^{-2}. a Coulombic efficiency plots. b-d The charge-discharge profiles at 1th (b), 30th (c) and 50th (d) cycles.

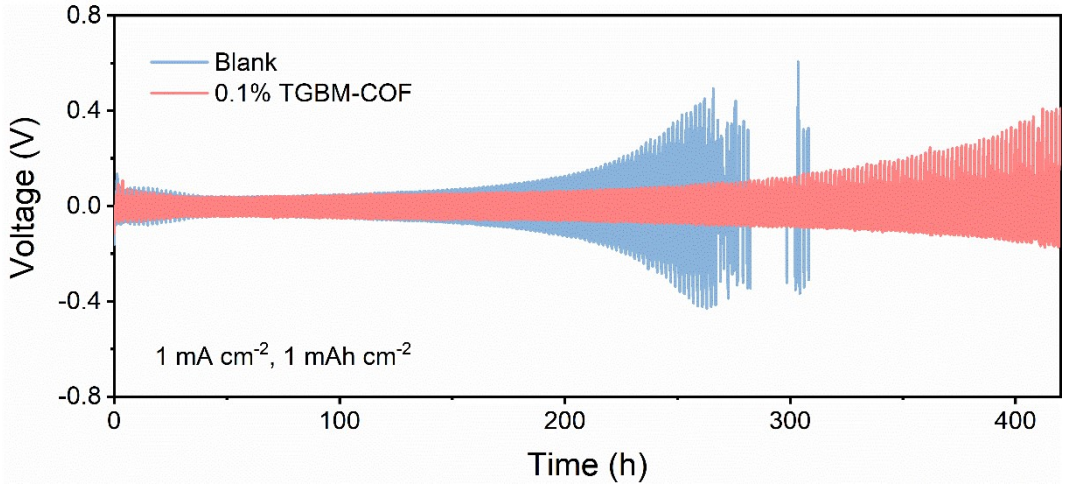

Figure S21. Cycling performances of Li symmetric cells using blank electrolyte and 0.1% TGBM-COF electrolyte at 1 mA cm^{-2} with 1 mAh cm^{-2}.

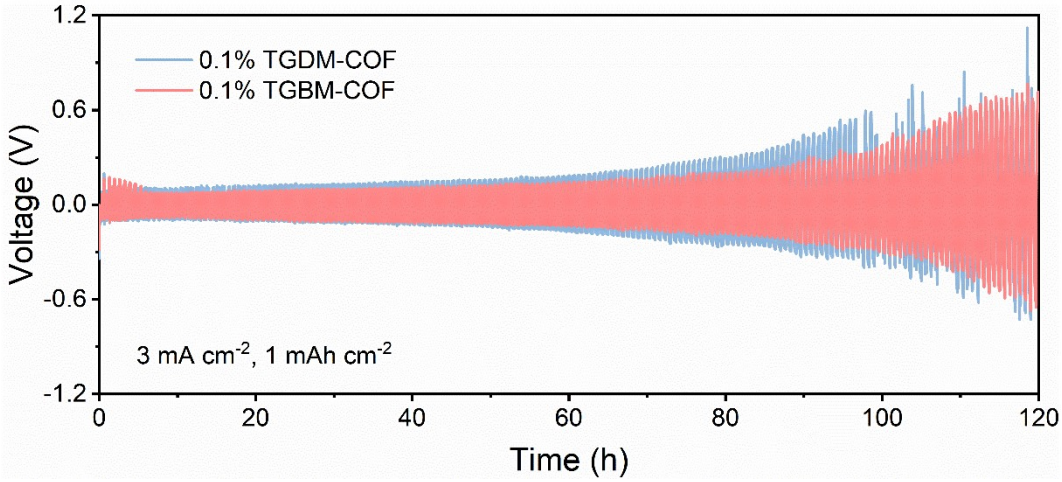

Figure S22. Cycling performances of Li symmetric cells using 0.1% TGDM-COF electrolyte and 0.1% TGBM-COF electrolyte at 3 mA cm^{-2} with 1 mAh cm^{-2}.

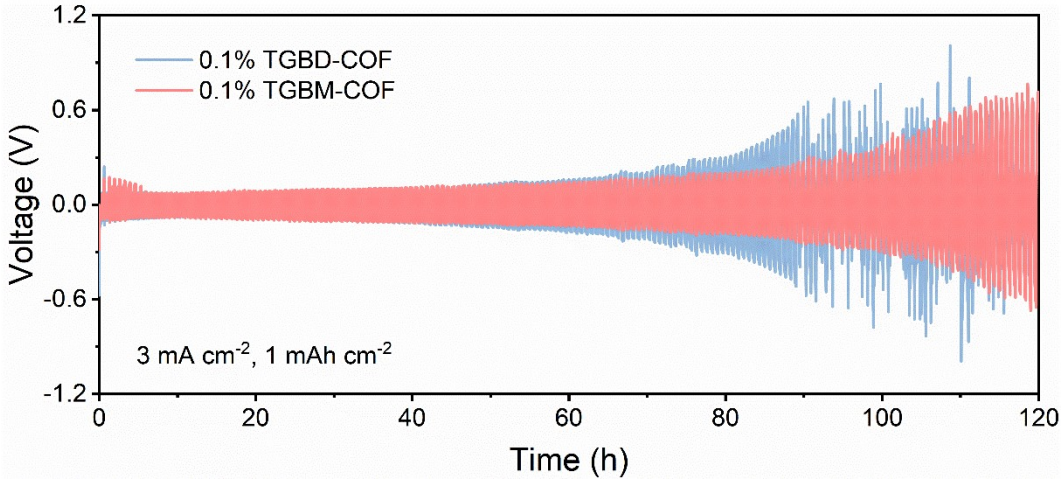

Figure S23. Cycling performances of symmetric cells using 0.1% TGBD-COF electrolyte and 0.1% TGBM-COF electrolyte at 3 mA cm^{-2} with 1 mAh cm^{-2}.

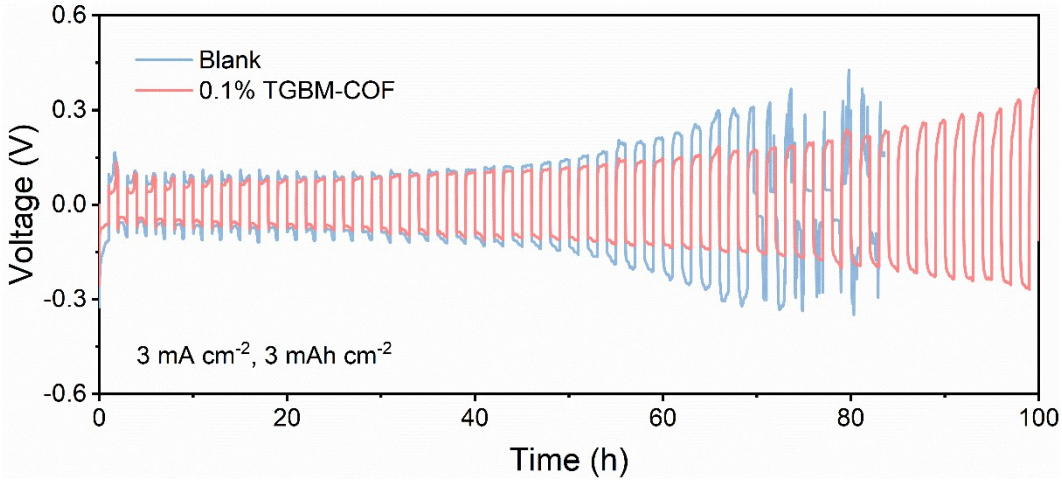

Figure S24. Cycling performances of Li symmetric cells using blank electrolyte and 0.1% TGBM-COF electrolyte at 3 mA cm^{-2} with 3 mAh cm^{-2}.

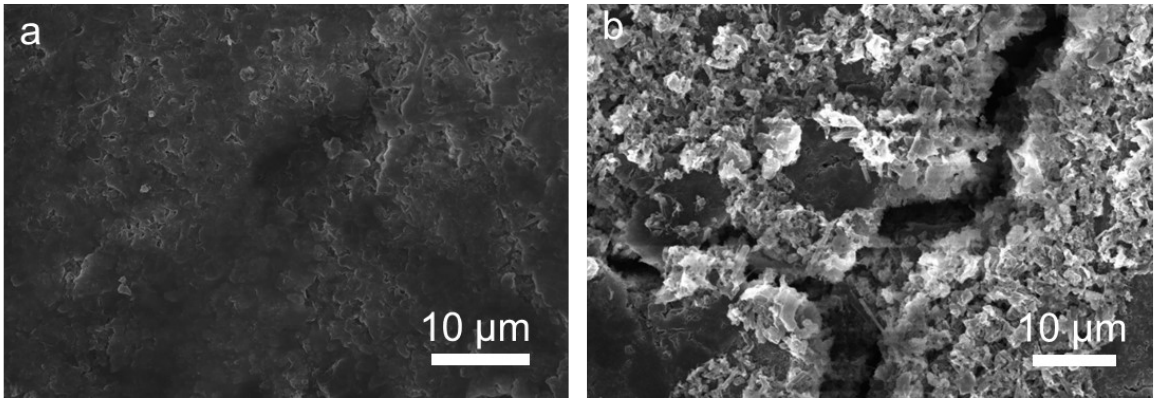

Figure S25. The SEM images of Li anodes using different electrolytes cycling at 3 mA cm^{-2} and 1 mAh cm^{-2} after 80 cycles. **a** 0.1% TGBM-COF electrolyte. **b** Blank electrolyte.

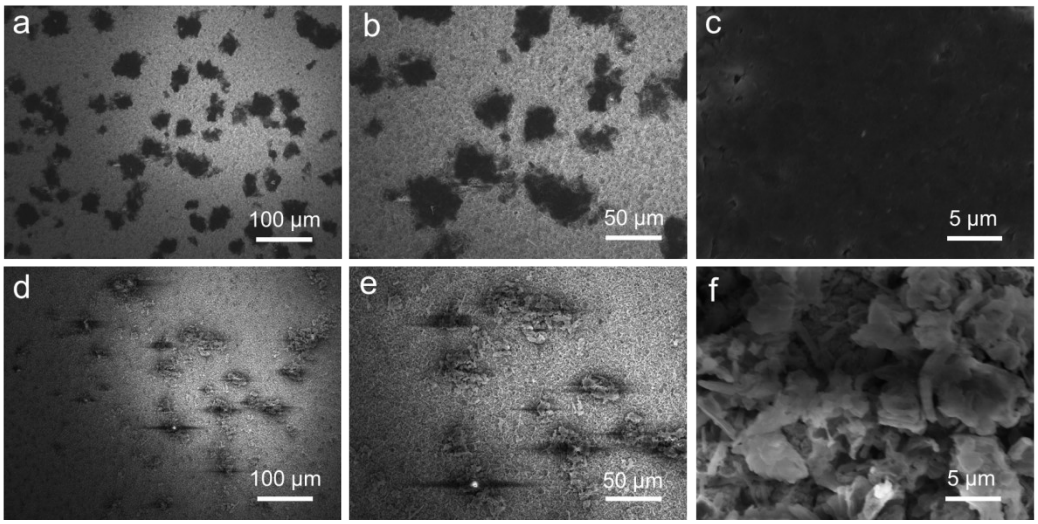

Figure S26. The SEM images of lithium plating on Cu foil using different electrolytes at 0.5 mA cm^{-2} for 0.5 h. a-c 0.1% TGBM-COF electrolyte. d-f Blank electrolyte.

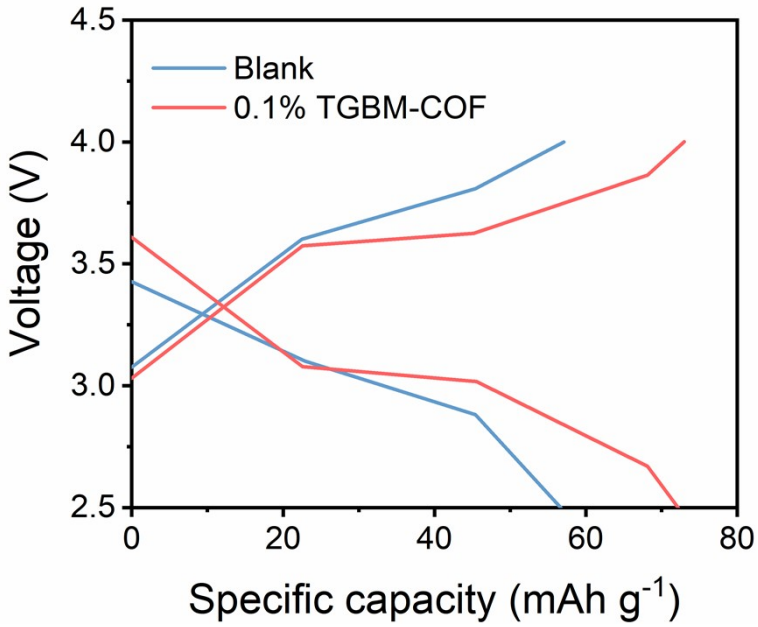

Figure S27. Galvanostatic charge-discharge profiles of full cells at 500 cycles at 8 C

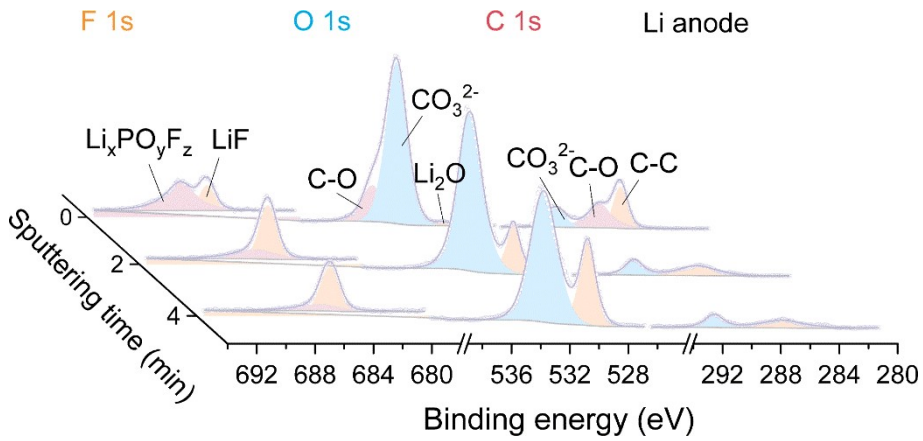

Figure S28. XPS depth profiles of C 1s, O 1s and F 1s of the SEI formed on Li anode with blank electrolyte after 10 cycles at 1 mA cm^{-2} and 1 mAh cm^{-2} with various Ar^+ sputtering time.

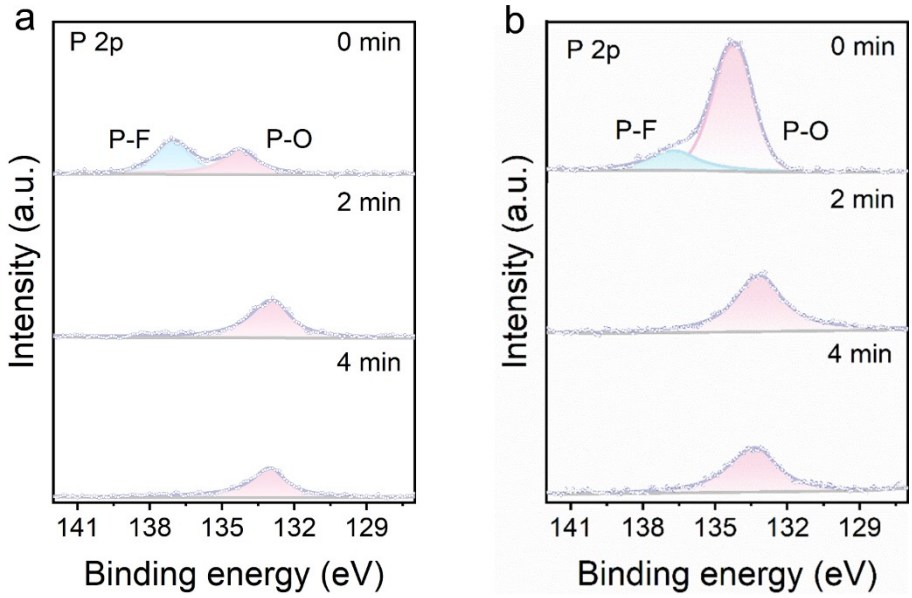

Figure S29. XPS depth profiles of P 2p of the SEI formed on Li anode after 10 cycles at 1 mA cm^{-2} and 1 mAh cm^{-2} with various Ar^{+} sputtering time. **a** Blank electrolyte. **b** 0.1% TGBM-COF electrolyte.

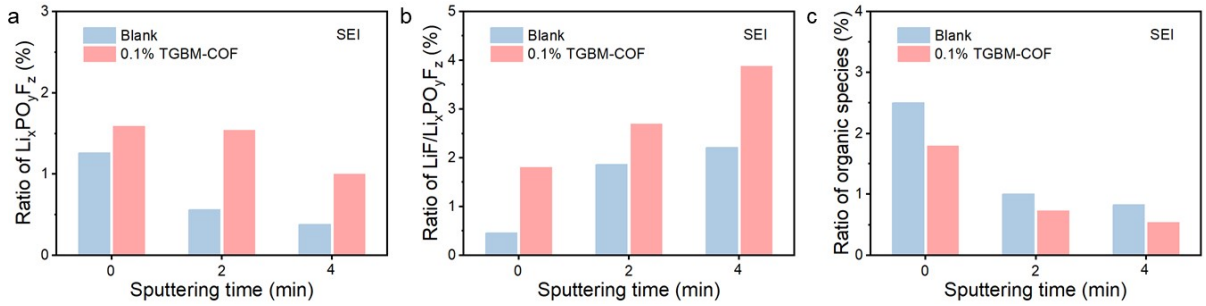

Figure S30. The ratio of $Li_xPO_yF_z$, $LiF/Li_xPO_yF_z$ and organic species in SEI with different electrolytes.

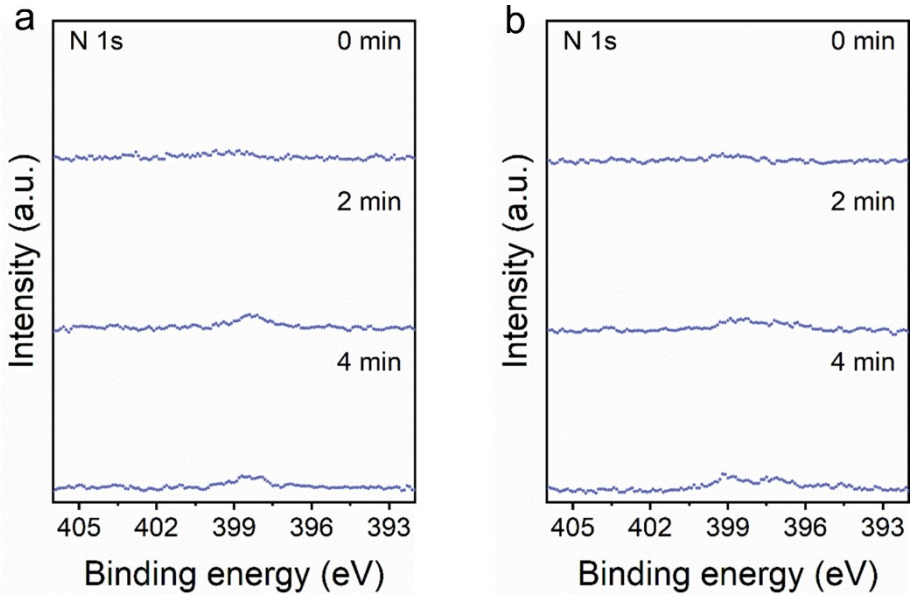

Figure S31. XPS depth profiles of N 1s of the SEI formed on Li anode after 10 cycles at 1 mA cm^{-2} and 1 mAh cm^{-2} with various Ar^{+} sputtering time. **a** Blank electrolyte. **b** 0.1% TGBM-COF electrolyte.

Figure S32. The optical image of transparaent cell.

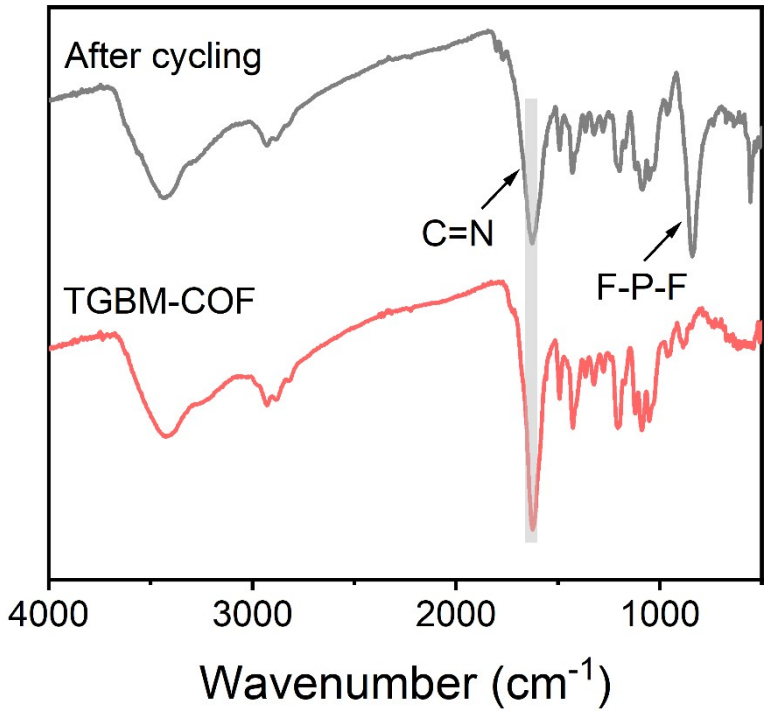

Figure S33. FT-IR spectra of TGBM-COF after cycling.

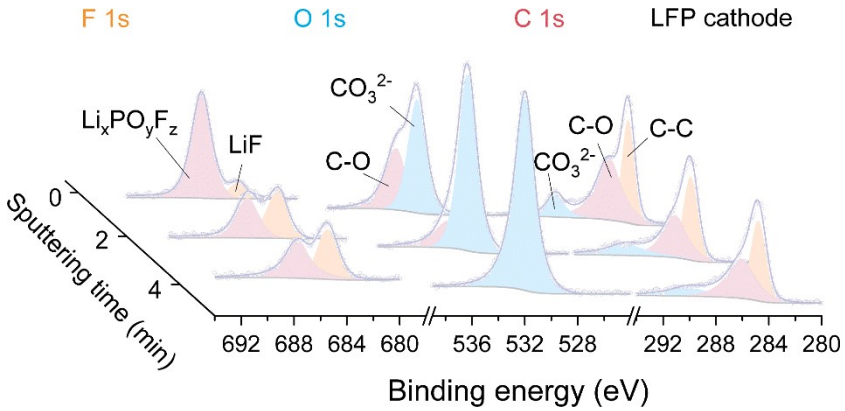

Figure S34. XPS depth profiles of C 1s, O 1s and F 1s of the CEI formed on LFP cathode with blank electrolyte after 10 cycles at 1 mA cm^{-2} and 1 mAh cm^{-2} with various Ar^+ sputtering time.

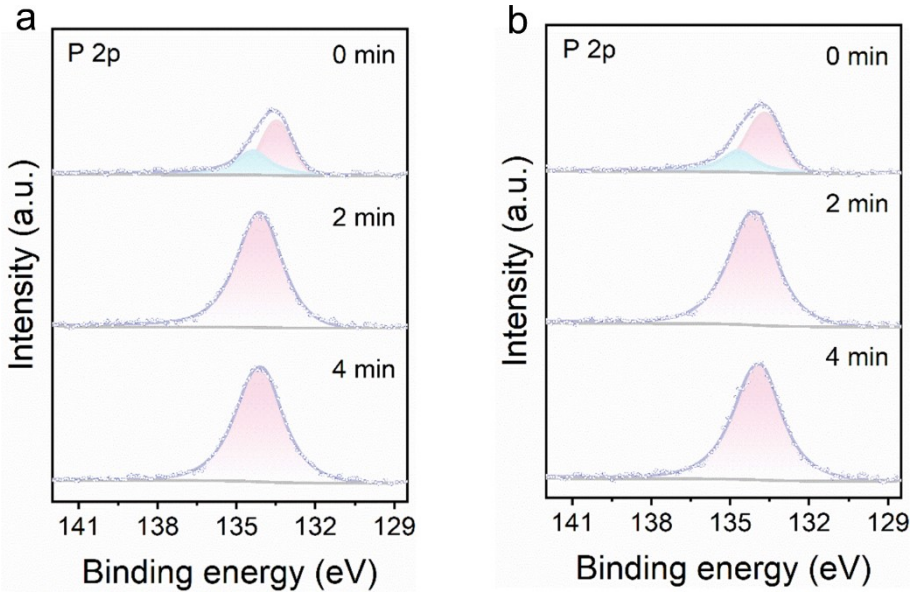

Figure S35. XPS depth profiles of P 2p of the CEI formed on LFP cathode after 10 cycles at 1 C with various Ar^+ sputtering time. **a** Blank electrolyte. **b** 0.1% TGBM-COF electrolyte.

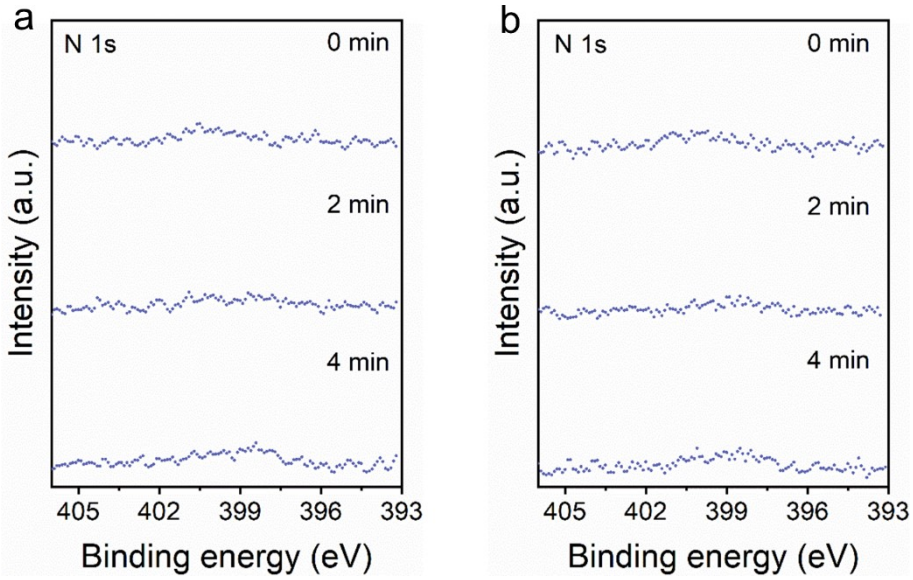

Figure S36. XPS depth profiles of N 1s of the CEI formed on LFP cathode after 10 cycles at 1 C with various Ar^+ sputtering time. **a** Blank electrolyte. **b** 0.1% TGBM-COF electrolyte.

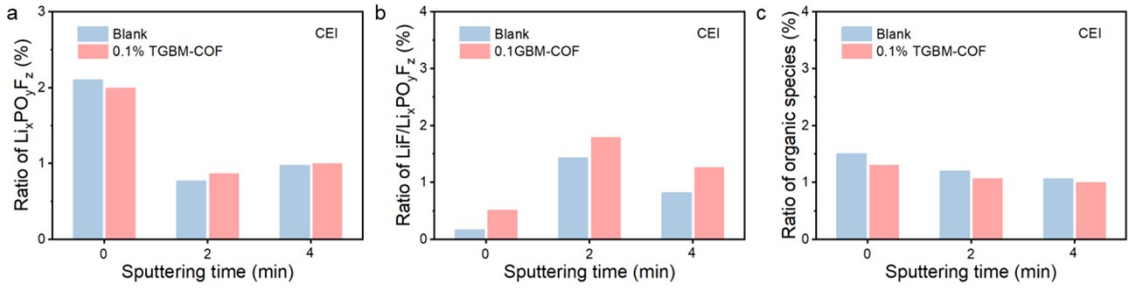

Figure S37. The ratio of $Li_xPO_yF_z$, $LiF/Li_xPO_yF_z$ and organic species in CEI with different electrolytes.

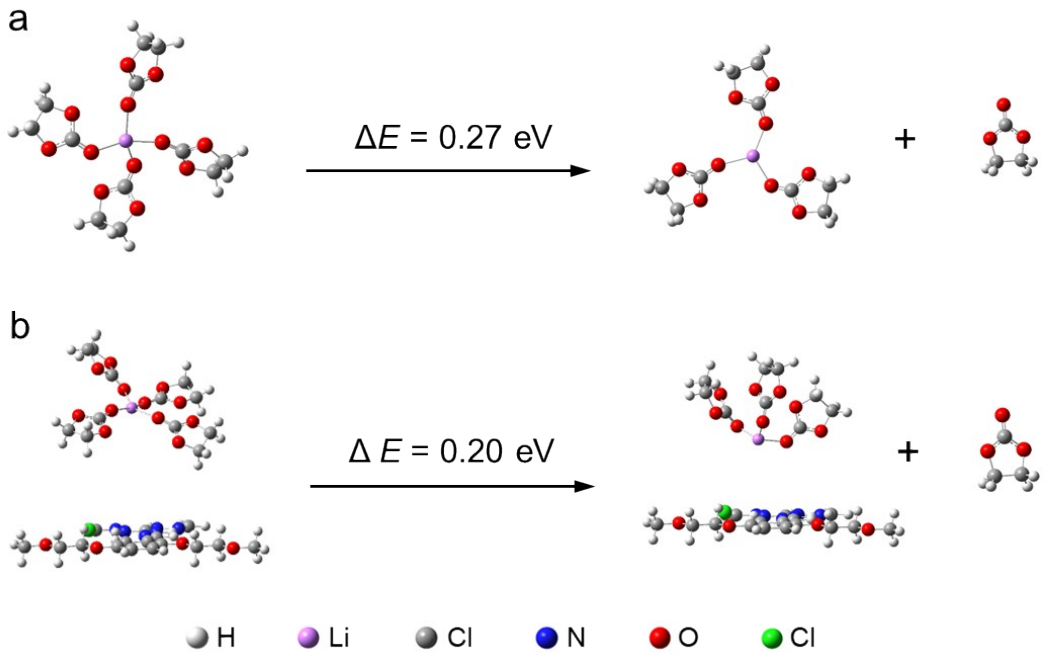

Figure S38. Li^+ de-solvation process ($Li(EC)_4^+$ to $Li(EC)_3^+$ and EC molecule) in different electrolytes. a Blank electrolyte. b 0.1% TGBM-COF electrolyte.

Table S1. Fractional atomic coordinates for the structure of AA stacking of TGBM-COF based on Materials Studio 2020 modeling program.

*P*6/m (175) Hexagonal			
$a = b = 20.7082$ Å, $c = 3.5160$ Å			
$\alpha = \beta = 90°$ and $\gamma = 120°$			
Atom	x/a	y/b	z/c
N1	-0.32564	0.40146	0.50000
N2	-0.20563	0.38373	0.50000
C3	-0.50978	0.92862	0.50000
C4	-0.43826	0.98973	0.50000
C5	-0.42940	0.06084	0.50000
C6	-0.47896	0.14638	0.50000
O7	-0.97782	0.64423	0.50000
C8	-0.04244	0.65024	0.50000
C9	-0.02076	0.73070	0.50000
O10	-0.08408	0.73644	0.50000
C11	-0.05782	0.81172	0.50000
C12	-0.33333	0.33333	0.50000

Table S2. Fractional atomic coordinates for the structure of AA stacking of TGDM-COF based on Materials Studio 2020 modeling program.

*P*6/m (175) Hexagonal			
$a = b = 20.8508$ Å, $c = 3.4300$ Å			
$\alpha = \beta = 90°$ and $\gamma = 120°$			
Atom	x/a	y/b	z/c
N1	-0.67457	0.59897	0.50000
N2	-0.58891	0.79727	0.50000
C3	-0.52357	0.85341	0.50000
C4	-0.92846	0.56035	0.50000
C5	-0.43950	0.98831	0.50000
C6	-0.42922	1.05955	0.50000
O7	-0.38040	0.97503	0.50000
C8	-0.30933	1.03833	0.50000
C9	-0.66667	0.66667	0.50000

Table S3. Fractional atomic coordinates for the structure of AA stacking of TGBD-COF based on Materials Studio 2020 modeling program.

*P*6/m (175) Hexagonal			
$a = b = 21.1155$ Å, $c = 3.5141$ Å			
$\alpha = \beta = 90°$ and $\gamma = 120°$			
Atom	x/a	y/b	z/c
N1	-0.28495	0.30470	0.50000
N2	-0.34659	0.44910	0.50000
C3	-0.42059	0.41549	0.50000
C4	-0.45932	0.08019	0.50000
C5	-0.42012	0.53948	0.50000
C6	0.54041	0.57993	0.50000
C9	-0.33333	0.33333	0.50000

Table S4. The current and resistance obtained before/after polarization for the calculation of Li^+ transference number.

	I_0 (mA)	I_s (mA)	R_0 (Ω)	R_s (Ω)	t_{Li+}
Blank	0.025	0.014	230.4	276.1	0.39
0.1% TGBM-COF	0.030	0.024	210	265	0.83

Table S5. Comparison of the performances of $LiFePO_4$ full cells using 0.1% TGBM-COF electrolyte and various reported materials.

Materials	Role	Loading	Current density (C)	Cycle number	Capacity retention (%)	Refs
$LiNO_3$ + CuF_2	Additive	6 mg cm^{-2}	0.5	400	80.0	[13]
FEC/$LiNO_3$	Additive	~6 mg cm^{-2}	1	1000	80.8	[14]
PDMS-OCH3	Additive	12 mg cm^{-2}	0.5	270	83.3	[15]
VS	Additive	1.5 mg cm^{-2}	0.5	150	96.2	[16]
ST-Li-E2	Additive	~7.5 mg cm^{-2}	1	200	85.0	[17]
OP-10	Additive	1.0-1.2 mg cm^{-2}	10	1000	74.5	[18]
TEOS/TEOT	Additive	0.9-1.2 mg cm^{-2}	10	3000	75.0	[19]
TMU/$LiNO_3$	Additive	3.53 mg cm^{-2}	1	550	94.6	[20]
CoPc	Additive	1.2 mg cm^{-2}	2	1000	96.4	[21]
Nano $CaCO_3$	Additive	6-7 mg cm^{-2}	1	250	87.0	[22]
DETFP	Additive	2.5 mg cm^{-2}	5	800	92.7	[23]
$In(NO_3)_3$	Additive	-	0.5	250	92.8	[24]
TF31	Additive	2 mg cm^{-2}	1	1000	96.4	[25]
ArFTFSI	Additive	~3 mg cm^{-2}	2	1000	48.0	[26]
HFT+$LiNO_3$	Additive	3 mg cm^{-2}	1	800	80.0	[27]
LNO-SE	Additive	4.3 mg cm^{-2}	2	1800	86.0	[28]
TpPa-Li	Coating	3.9 mg cm^{-2}	1	350	95.5	[29]
S-COF@Li	Coating	4 mg cm^{-2}	0.5	250	88.9	[30]
TpTG Li	Coating	3.5 mg cm^{-2}	0.5	180	72.2	[31]
NO_2-COF@Li	Coating	3.2 mg cm^{-2}	1	1000	91	[32]
sp^2c-COF-Co@Li	Coating	4 mg cm^{-2}	1	650	-	[33]
sp^2c-COF@Li	Coating	4 mg cm^{-2}	1	500	-	[34]
TGBM-COF	Additive	**~3 mg cm^{-2}**	**8**	500 900	**88.2** **76.2**	**This work**

Table S6. Comparison of the performances of full cells using TGBM-COF and various reported COFs as electrolyte additive for full cells.

Materials	Cathode	Loading	Anode	Current density (C)	Cycle number	Capacity retention (%)	Refs
TpTta COF	NCM811	3.6 mg cm^{-2}	Li	0.5	100	87.1	[35]
Py-Bpy-Br COF	NMC622	4.64 mg cm^{-2}	Si/C	10	400	92.4	[36]
COF-TAP-4EO	S	-	Li	0.2	100	91.9	[37]
TGBM-COF	**LFP**	**~3 mg cm^{-2}**	**Li**	**8**	500	**88.2**	**This work**

Reference

1. A.D. Becke Density-functional thermochemistry. III. The role of exact exchange. *J. Chem. Phys.* 1993, **98**, 5648-5652.
2. M.J. Frisch, G.W. Trucks, H.B. Schlegel, G.E. Scuseria, M.A. Robb, J.R. Cheeseman, G. Scalmani, V. Barone, G.A. Petersson, H. Nakatsuji, X. Li, M. Caricato, A.V. Marenich, J. Bloino, B.G. Janesko, R. Gomperts, B. Mennucci, H.P. Hratchian, J.V. Ortiz, A.F. Izmaylov, J.L. Sonnenberg, Williams, F. Ding, F. Lipparini, F. Egidi, J. Goings, B. Peng, A. Petrone, T. Henderson, D. Ranasinghe, V.G. Zakrzewski, J. Gao, N. Rega, G. Zheng, W. Liang, M. Hada, M. Ehara, K. Toyota, R. Fukuda, J. Hasegawa, M. Ishida, T. Nakajima, Y. Honda, O. Kitao, H. Nakai, T. Vreven, K. Throssell, J.A. Montgomery Jr., J.E. Peralta, F. Ogliaro, M.J. Bearpark, J.J. Heyd, E.N. Brothers, K.N. Kudin, V.N. Staroverov, T.A. Keith, R. Kobayashi, J. Normand, K. Raghavachari, A.P. Rendell, J.C. Burant, S.S. Iyengar, J. Tomasi, M. Cossi, J.M. Millam, M. Klene, C. Adamo, R. Cammi, J.W. Ochterski, R.L. Martin, K. Morokuma, O. Farkas, J.B. Foresman & D.J. Fox (Wallingford, CT; 2016).
3. A.V. Marenich, C.J. Cramer & D.G. Truhlar Universal solvation model based on solute electron density and on a continuum model of the solvent defined by the bulk dielectric constant and atomic surface tensions. *J. Phys. Chem. B* 2009, **113**, 6378–6396.
4. S. Grimme, J. Antony, S. Ehrlich & H. Krieg A consistent and accurateab initioparametrization of density functional dispersion correction (DFT-D) for the 94 elements H-Pu. *J. Chem. Phys.* 2010, **132**, 154104.
5. P.C. Hariharan & J.A. Pople The influence of polarization functions on molecular orbital hydrogenation energies. *Theoret. chim. Acta* 1973, **28**, 213-222.
6. P.J. Hay & W.R. Wadt Ab initio effective core potentials for molecular calculations. Potentials for K to Au including the outermost core orbitals. *J. Chem. Phys.* 1985, **82**, 299-310.
7. M. Meunier & S. Robertson Materials Studio 20th anniversary. *Mol. Simulat.* 2021, **47**, 537-539.
8. C. Kutzner, S. Páll, M. Fechner, A. Esztermann, B.L. de Groot & H. Grubmüller More bang for your buck: Improved use of GPU nodes for GROMACS 2018. *J. Comput. Chem.* 2019, **40**, 2418-2431.
9. J. Wang, R.M. Wolf, J.W. Caldwell, P.A. Kollman & D.A. Case Development and testing of a general amber force field. *J. Comput. Chem.* 2004, **25**, 1157–1174.
10. K.G. Sprenger, V.W. Jaeger & J. Pfaendtner The general AMBER force field (GAFF) can accurately predict thermodynamic and transport properties of many ionic liquids. *J. Phys. Chem. B* 2015, **119**, 5882-5895.
11. J.K. Johnson, J.A. Zollweg & K.E. Gubbins The Lennard-Jones equation of state revisited. *Mol. Phys.* 2006, **78**, 591-618.
12. U. Essmann, L. Perera, M.L. Berkowitz, T. Darden, H. Lee & L.G. Pedersen A smooth particle mesh Ewald method. *J. Chem. Phys.* 1995, **103**, 8577-8593.
13. C. Yan, Y.X. Yao, X. Chen, X.B. Cheng, X.Q. Zhang, J.Q. Huang & Q. Zhang Lithium nitrate solvation chemistry in carbonate electrolyte sustains high-voltage lithium metal batteries. *Angew. Chem. Int. Ed.* 2018, **57**, 14055-14059.
14. X.Q. Zhang, X. Chen, X.B. Cheng, B.Q. Li, X. Shen, C. Yan, J.Q. Huang & Q. Zhang Highly stable lithium metal batteries enabled by regulating the solvation of lithium ions in nonaqueous electrolytes. *Angew. Chem. Int. Ed.* 2018, **57**, 5301-5305.
15. J. Meng, F. Chu, J. Hu & C. Li Liquid polydimethylsiloxane grafting to enable dendrite-free Li plating for highly reversible Li-metal batteries. *Adv. Funct. Mater.* 2019, **29**, 1902220.
16. Q. Ma, X. Sun, P. Liu, Y. Xia, X. Liu & J. Luo Bio-inspired stable lithium-metal anodes

by co-depositing lithium with a 2D vermiculite shuttle. *Angew. Chem. Int. Ed.* 2019, **58**, 6200-6206.
17. J. Zhuang, X. Wang, M. Xu, Z. Chen, M. Liu, X. Cheng & W. Li A self-healing interface on lithium metal with lithium difluoro (bisoxalato) phosphate for enhanced lithium electrochemistry. *J. Mater. Chem. A* 2019, **7**, 26002-26010.
18. H. Dai, X. Gu, J. Dong, C. Wang, C. Lai & S. Sun Stabilizing lithium metal anode by octaphenyl polyoxyethylene-lithium complexation. *Nat. Commun.* 2020, **11**, 643.
19. Y. Zhong, P. Huang, W. Yan, Z. Su, C. Sun, Y. Xing & C. Lai Ion-conductive polytitanosiloxane networks enable a robust solid-electrolyte interface for long-cycling lithium metal anodes. *Adv. Funct. Mater.* 2021, **32**, 2110347.
20. Z. Piao, P. Xiao, R. Luo, J. Ma, R. Gao, C. Li, J. Tan, K. Yu, G. Zhou & H.M. Cheng Constructing a stable interface layer by tailoring solvation chemistry in carbonate electrolytes for high-performance lithium-metal batteries. *Adv. Mater.* 2022, **34**, 2108400.
21. H. Dai, J. Dong, M. Wu, Q. Hu, D. Wang, L. Zuin, N. Chen, C. Lai, G. Zhang & S. Sun Cobalt-phthalocyanine-derived molecular isolation layer for highly stable lithium anode. *Angew. Chem. Int. Ed.* 2021, **60**, 19852-19859.
22. Q. Peng, Z. Liu, L. Jiang & Q. Wang Optimized cycle and safety performance of lithium–metal batteries with the sustained-release effect of nano CaCO3. *Adv. Energy Mater.* 2022, **12**, 2104021.
23. P. Zhou, Y. Xia, W.-h. Hou, S. Yan, H.-Y. Zhou, W. Zhang, Y. Lu, P. Wang & K. Liu Rationally designed fluorinated amide additive enables the stable operation of lithium metal batteries by regulating the interfacial chemistry. *Nano Lett.* 2022, **22**, 5936-5943.
24. A.G. Paul-Orecchio, L. Stockton, J.A. Weeks, A. Dolocan, Y. Wang & C.B. Mullins Alloying indium additive enables fast-charging lithium metal batteries. *ACS Energy Lett.* 2023, **8**, 4228-4234.
25. C. Liao, L. Han, W. Wang, W. Li, X. Mu, Y. Kan, J. Zhu, Z. Gui, X. He, L. Song & Y. Hu Non-flammable electrolyte with lithium nitrate as the only lithium salt for boosting ultra-stable cycling and fire-safety lithium metal batteries. *Adv. Funct. Mater.* 2023, **33**, 2212605.
26. K. Peng, P. Tang, Q. Yao, Q. Dou & X. Yan Bifunctional fluoropyridinium-based cationic electrolyte additive for dendrite-free Li metal anode. *Nano Res.* 2023, **16**, 9530-9537.
27. J. Jiang, M. Li, X. Liu, J. Yi, Y. Jiang, C. Wu, H. Liu, B. Zhao, W. Li, X. Sun, J. Zhang & S. Dou Multifunctional additives to realize dendrite-free lithium deposition in carbonate electrolytes toward low-temperature Li metal batteries. *Adv. Energy Mater.* 2024, **14**, 2400365.
28. F. Mushtaq, H. Tu, L. Zhao, L. Wang, B. Tang, Z. He, Y. Cao, Z. Hou, J. Ran, J. Wang, M. Zahid, Y. Zhang & M. Liu Dielectric additive induced weak Li solvation towards stabilized solid electrolyte interface for 4.6V lithium metal batteries. *Energy Storage Mater.* 2024, **73**, 103854.
29. D. Chen, P. Liu, L. Zhong, S. Wang, M. Xiao, D. Han, S. Huang & Y. Meng Covalent Organic Frameworks with Low Surface Work Function Enabled Stable Lithium Anode. *Small* 2021, **17**.
30. W. Wang, Z. Yang, Y. Zhang, A. Wang, Y. Zhang, L. Chen, Q. Li & S. Qiao Highly stable lithium metal anode enabled by lithiophilic and spatial-confined spherical-covalent organic framework. *Energy Storage Mater.* 2022, **46**, 374-383.
31. Y. Zhang, W. Wang, M. Hou, Y. Zhang, Y. Dou, Z. Yang, X. Xu, H. Liu & S. Qiao Self-exfoliated covalent organic framework nano-mesh enabled regular charge distribution for highly stable lithium metal battery. *Energy Storage Mater.* 2022, **47**, 376-385.
32. Y. Yang, C. Zhang, G. Zhao, Q. An, Z.y. Mei, Y. Sun, Q. Xu, X. Wang & H. Guo

Regulating the Electron Structure of Covalent Organic Frameworks by Strong Electron-Withdrawing Nitro to Construct Specific Li+ Oriented Channel. *Adv. Energy Mater.* 2023, **13**.

33. C. Zhang, J. Xie, C. Zhao, Y. Yang, Q. An, Z. Mei, Q. Xu, Y. Ding, G. Zhao & H. Guo Regulating the Lithium Ions' Local Coordination Environment through Designing a COF with Single Atomic Co Site to Achieve Dendrite-Free Lithium-Metal Batteries. *Adv. Mater.* 2023, **35**, e2304511.
34. C. Zhang, Y. Yang, Y. Sun, L. Duan, Z. Mei, Q. An, Q. Jing, G. Zhao & H. Guo 2D sp2-carbon-linked covalent organic frameworks as artificial SEI film for dendrite-free lithium metal batteries. *Sci. China Mater.* 2023, **66**, 2591-2600.
35. W. Zhang, G. Jiang, W. Zou, X. Chen, S. Peng, S. Qi, R. Hu, H. Song, Z. Cui, L. Du & Z. Liang A microscopically heterogeneous colloid electrolyte of covalent organic nanosheets for ultrahigh-voltage and low-temperature lithium metal batteries. *Energy Environ. Sci.* 2024, **17**, 2642-2650.
36. W. Zhang, W. Zou, G. Jiang, S. Qi, S. Peng, H. Song, Z. Cui, Z. Liang & L. Du A microscopically heterogeneous colloid electrolyte for extremely fast-charging and long-calendar-life silicon-based lithium-ion batteries. *Angew. Chem. Inter. Ed.* 2024, **63**, e202410046.
37. C. Guo, P. Xue, W. Feng, Y. Yang, L. Zhou, H. Zhuang, Y. Chen, Y. Chen & Y.Q. Lan Covalent organic framework quantum dots for near-frictionless ion transport battery electrolyte. *Angew. Chem. Inter. Ed.* 2025, **64**, e202512031.